CHALMERS
UNIVERSITY OF TECHNOLOGY

Design and Characterization of In0.22Ga0.78As-based Schottky-barrier diode mixers operating at 3.4 THz

Citation for the original published paper (version of record):
Jayasankar, D., Rothbart, N., Reck, T. et al (2026). Design and Characterization of In0.22Ga0.78As-based Schottky-barrier diode mixers operating at 3.4 THz. IEEE Transactions on Terahertz Science and Technology, In Press.
http://dx.doi.org/10.1109/TTHZ.2026.3683530

(article starts on next page)

Design and Characterization of $In_{0.22}Ga_{0.78}As$-based Schottky-barrier diode mixers operating at 3.4 THz

Divya Jayasankar, *Member, IEEE*, Nick Rothbart, Theodore Reck, Jan Stake, *Fellow, IEEE*, Jeffrey Hesler†, and Heinz-Wilhelm Hübers

***Abstract*—A key challenge in developing terahertz Schottky-barrier diode-based receivers operating at ambient temperatures is to overcome the complexities of fabrication and machining, and to achieve efficient coupling between the waveguide feed horn and the THz signal. This paper presents characterization of WM-57, $In_{0.22}Ga_{0.78}As$ Schottky-barrier diode mixers realized on a 2-μm-thin AlGaAs membrane. The mixers were pumped by a quantum-cascade laser operating at 3.4 THz; the radio and local-oscillator signals were spatially superimposed using a Mylar beam splitter and coupled to the mixers via an integrated pyramidal horn antenna. A double-sideband receiver noise temperature of 28 500 K was measured at 3.4 THz for 6-μm Mylar at an IF of 1.5 GHz, with 2-mW of LO power coupled to the mixer. The DSB receiver noise temperature corrected for atmospheric attenuation is 27 600 K. These results represent a key step toward room-temperature THz front-end systems for limb-sounding instruments to detect trace gases in the mesosphere and lower thermosphere of the Earth's atmosphere.**

***Index Terms*—Far-infrared, Heterodyne receivers, InGaAs, Mixers, Schottky-barrier diodes, Terahertz electronics.**

I. Introduction

SCHOTTKY-barrier diode technology plays a crucial role in broadband sub-millimeter wave heterodyne radiometers, particularly for applications that require ambient temperature operation [1]. Scientific goals and instrument requirements for Earth observation are driven by the need to measure hydroxyl radical (OH) and atomic oxygen (OI) lines at 3.5 THz and 4.7 THz, respectively, as well as to collect data over extended periods, for example a full solar cycle (11 years) [2]–[4]. This creates significant demand for compact, high-resolution terahertz heterodyne receivers that operate without cryogenic cooling. Compared to ultra-low-noise superconducting mixers such as superconductor-insulator-superconductor (SIS) and hot-electron bolometer (HEB) mixers, Schottky diodes offer the advantage of operating over a broad temperature range and a large intermediate frequency (IF) bandwidth, making them ideal for long-duration missions. GaAs-based Schottky receivers have been the workhorses behind several space missions, including ODIN [5], MIRO [6], ISMAR [7], METOP, JUICE [8], [9], and AWS [10]. More recently, Maestrini *et al.* [11] demonstrated a bias-able, anti-parallel GaAs Schottky diodes exhibiting a double side-band (DSB) receiver noise temperature of 6000 K at 2.06 THz. Despite this progress, the development of Schottky-based mixers operating above 3 THz with good sensitivity remains a challenge, see Fig. 1.

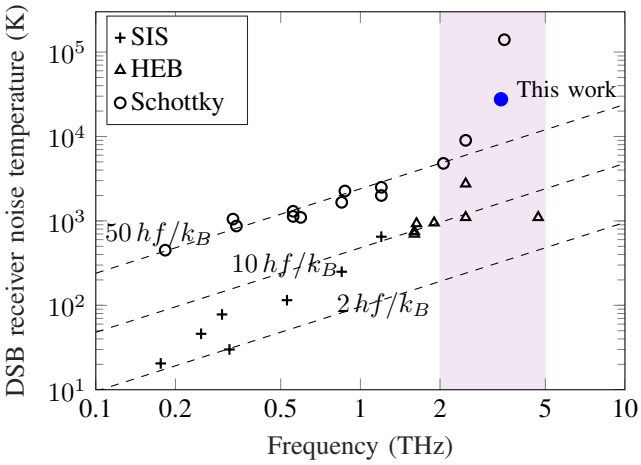

Fig. 1: State-of-the-art THz mixers. Planar Schottky data is from [7], [8], [11]–[19], and the superconducting HEB and SIS mixers are from [20]. Note: hf/k_B is the quantum limit where h is Planck's constant, f frequency, and k_B Boltzmann's constant.

Several key fabrication challenges persist in realizing planar integrated mixer circuitry on ultra-thin III-V substrates, as well as precision machining of THz mixer waveguide blocks with tolerances better than ± 1 μm. High local oscillator (LO) power requirements to adequately pump the GaAs mixer impose constraints, especially above 3 THz. Previously, we reported a 3.5 THz single-ended GaAs Schottky mixer integrated with a diagonal horn. The LO signal from the quantum-cascade laser (QCL) was spatially superimposed with the radio-frequency (RF) signal using a Martin-Puplett diplexer, resulting in an

Manuscript received Feb 4 2026; revised Mar 2026; accepted xxxx. Date of publication xxxx; date of current version xxxx. This work was funded by Deutsche Forschungsgemeinschaft (DFG, German Research Foundation) - project number 468535812. *(Corresponding author: Divya Jayasankar)*, e-mail: divya.jayasankar@dlr.de

D. Jayasankar is with the German Aerospace Center (DLR), Institute for Space Research, 12489 Berlin, Germany, and also with the Terahertz and Millimetre Wave Laboratory, Department of Microtechnology and Nanoscience (MC2), Chalmers University of Technology, SE-412 96 Gothenburg, Sweden.

N. Rothbart is with the German Aerospace Center (DLR), Institute for Space Research, 12489 Berlin, Germany.

T. Reck is with the Virginia Diodes Inc. (VDI), Charlottesville, VA 22902 USA.

J. Stake is with the Terahertz and Millimeter Wave Laboratory, Department of Microtechnology and Nanoscience (MC2), Chalmers University of Technology, SE-412 96 Gothenburg, Sweden.

H.-W. Hübers is with the German Aerospace Center (DLR), Institute for Space Research and Humboldt-Universität zu Berlin, Department of Physics, 12489 Berlin, Germany.

J. Hesler† Deceased (Oct 2025).

Color versions of one or more figures in this article are available online at http://ieeexplore.ieee.org. Digital Object Identifier 10.1109/TTHZ.2024.xx

optical path length of about 80 cm. After correcting for atmospheric loss, the DSB receiver noise temperature was 140 000 K [19]. The excess loss was attributed to inefficient LO/RF power coupling [21] and waveguide loss.

In this work, we present the development and characterization of $In_{0.22}Ga_{0.78}As$ Schottky barrier diode mixers with an integrated pyramidal horn [21] operating at 3.4 THz. InGaAs is a compound semiconductor that has a higher electron affinity (χ_s) and a narrower bandgap than GaAs, which leads to a lower Schottky-barrier height (Φ_b), thereby relaxing the LO pump power requirements [22], [23]. With a low barrier height, the saturation current is higher, resulting in a lower knee voltage. InGaAs also exhibits higher mobility and carrier velocity than GaAs, but the surface interface physics between metal and a ternary semiconductor is complicated.

In this paper, we present the characterisation of two identical $In_{0.22}Ga_{0.78}As$ mixers to assess repeatability of fabrication and assembly processes in an optimized measurement setup, improving upon our prior preliminary study [24]. The QCL-LO and RF signals were coupled to the mixer via a Mylar beamsplitter, enabling a compact receiver breadboard. We present a comprehensive assessment of the mixers' performance using Mylar beam splitters of varying thicknesses in different IF bands.

The paper is organized as follows: Section II presents the design and fabrication of the InGaAs mixers. Section III describes the frequency and power characterization of the QCL. Followed by the coupling of the LO signal to the mixer, including analytical Gaussian beam coupling simulations, and experimental evaluation of Mylar beam splitters and their efficiency in directing QCL and RF signals to the mixer. Following this, the experimental setup for RF mixer characterization and results are presented in Sections IV and V.

II. Mixer Design and Fabrication

This section presents the three-dimensional electromagnetic (3D-EM) model of the mixer, the fabrication process of the planar, integrated mixer circuitry, and the final assembled mixer block with integrated pyramidal horn.

A. WM-57 Schottky mixers

The 3D-EM model of the $In_{0.22}Ga_{0.78}As$ mixer design is shown in Fig. 2. Single-ended diode topology was chosen for ease of fabrication. The mixer can operate both as a fundamental and a $\times$4-harmonic mixer. For the latter, the mixer can be pumped with a solid-state multiplier source operating at 1 THz, and the LO signal is coupled via WM-164 waveguide. In this work, the mixer is operated as a fundamental mixer, i.e., both the RF and LO signals are coupled via the integrated pyramidal horn and WM-57 waveguide to the diode as shown in Fig. 2. S_{11} of the pyramidal horn is better than 30 dB across the full waveguide band (3.3-5 THz). The diode embedding impedance at 3.4 THz is about $36+26j$ Ω. A ground beamlead near the diode is also required in this design to support broadband coupling of the LO and IF to the diode.

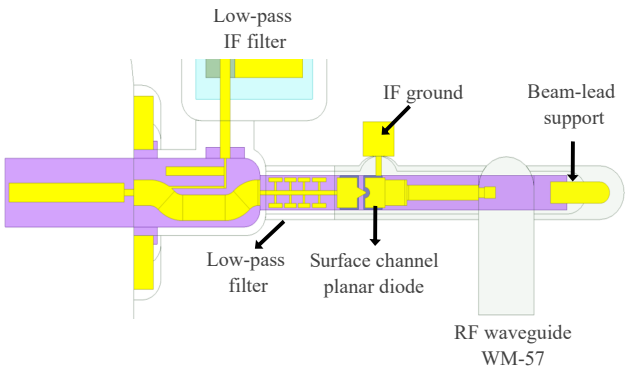

Fig. 2: Mixer design. 3D-EM model of the $In_{0.22}Ga_{0.78}As$ WM-57 mixer.

Fabrication of InGaAs mixer circuits was carried out at VDI using a standard Schottky MMIC process on a 2-μm-thin AlGaAs membrane using photolithography. It features a surface-channel planar diode with 0.5 μm anode diameter [25] and n-type semiconductor doping concentration of 5×10^{17} cm^{-3}. The micrograph of the fabricated mixer circuitry after release from the supporting substrate is shown in Fig. 3. The anode diameter was verified by removing the AlGaAs membrane and by scanning electron micrograph (SEM) of three devices. Once the mixer circuits are released from the supporting membrane, they are mounted inside a gold-plated, CNC-machined E-plane split-metal enclosure.

In this work, the mixers are packaged in a housing with a pyramidal horn, which is less sensitive to E-plane block misalignment due to its single-moded operation [21]. Fig. 4 shows the rectangular aperture (432 μm $\times$ 205 μm) of the pyramidal horn. Based on Gaussian beam coupling [26], the optimum beam waist for this pyramidal horn is about 150 μm. The simulated DSB mixer conversion loss was approximately 7 dB at 3.4 THz for an IF of 1.5 GHz, LO power of 2 mW, and bias current 0.9 mA, refer to Fig. 5. A standard diode model was employed, with an estimated series resistance of $R_s = 25\ \Omega$, junction capacitance of 0.6 fF, saturation current $I_{sat} = 15\ \mu$A, and ideality factor of 1.55. Junction capacitance is estimated by including the first-order fringing effects, due to curvature of the n-layer potential near the periphery of the anode, refer to [27]. In the initial modeling, a simple model was used for series resistance estimation, excluding

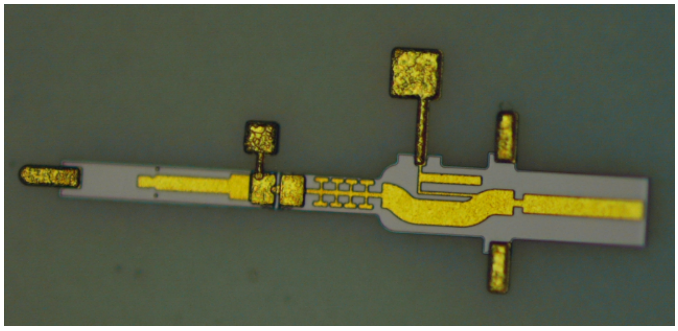

Fig. 3: Micrograph of the integrated $In_{0.22}Ga_{0.78}As$ mixer.

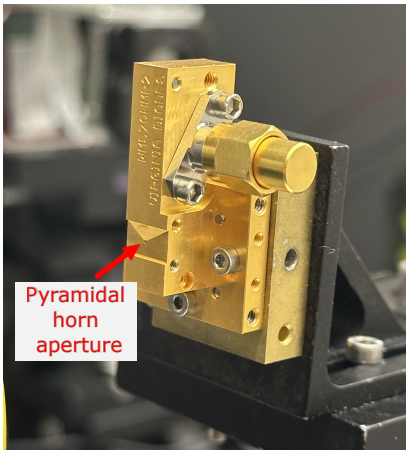

Fig. 4: Photograph of the assembled mixer block indicating the pyramidal horn aperture (432 μm $\times$ 205 μm).

high-frequency losses [28].

Only simulations of conversion loss are performed to simplify the harmonic-balance (HB) analysis. These simulations predict $T_m = T_{diode}(L_m - 1)$, where L_m is the conversion loss of the mixer, T_m is mixer noise temperature and T_{diode} is the effective diode temperature at the IF while diode is pumped by the LO and dc-biased [29]. The effective diode temperature includes the thermal and shot noise [30]–[32].

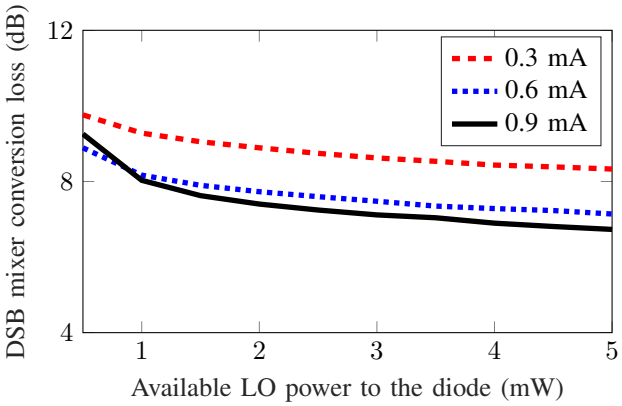

Fig. 5: Mixer simulation. Simulated DSB mixer conversion loss versus available LO power to the diode.

III. LO COUPLING

This section provides a brief description of the 3.4-THz QCL and micro-optical bench design. Followed by the frequency and power characterization of the QCL. In the latter part of the section, we estimate the power coupled into the mixer from the QCL-LO, taking into account coupling efficiency, atmospheric attenuation, optical component losses, and polarization effects.

A. Micro-integrated QCL characterization

The micro-integrated QCL comprises a silicon (Si) immersion lens, a $\lambda/4$ waveplate, and a wire grid as a linear polarizer to minimize back-reflections of the QCL emission

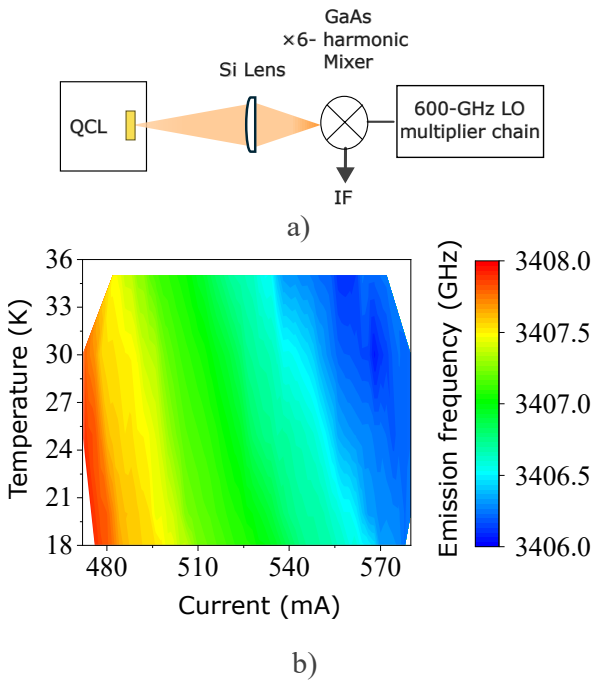

Fig. 6: Frequency characterization of the micro QCL. a) Schematic of the experimental setup (not to scale) b) QCL emission frequency for different QCL operating currents and temperatures.

and reduce optical feedback. All components are integrated on a compact 22 mm $\times$ 8 mm submount made of Copper (Cu). The QCL was designed and fabricated at the Paul-Drude-Institut (PDI), and the QCLs were assembled in the optical bench at Ferdinand-Braun-Institut (FBH). A detailed description of the QCL and micro-optical bench design is provided in [33]. The active region of the QCL is based on GaAs/AlAs heterostructures; further details are provided in [34]. The micro-QCL is soldered to a copper submount, which in turn is attached to the cold finger of a Gifford-McMahon cooler from Sumitomo (SRDK-408D).

The frequency characterization of the QCL was carried out using a GaAs-based Schottky diode-harmonic mixer from Chalmers University of Technology [35]. The incoming signal from the QCL is coupled via an external Si lens to the harmonic mixer, and the mixer is pumped by a 600-GHz LO multiplier chain from VDI as illustrated in the schematic Fig. 6a. The IF signal generated upon mixing with the $\times$6-harmonic of the LO signal is monitored via a spectrum analyzer, and the QCL frequency was determined by RF $= 6 \times$ LO $\pm$ IF, and the sideband is determined by LO signal tuning. Variation of the QCL emission frequency over different operating temperatures and bias currents is presented in Fig. 6b.

The optical output power of the QCL was measured using an absolute THz power meter from Thomas Keating (TK) Instruments. For detailed information on power meter calibration and frequency-dependent window loss correction, refer to the operating manual [36]. The output power measured in front of the cryocooler vacuum window is 23 mW for the QCL operating point: 550 mA bias current and a temperature of

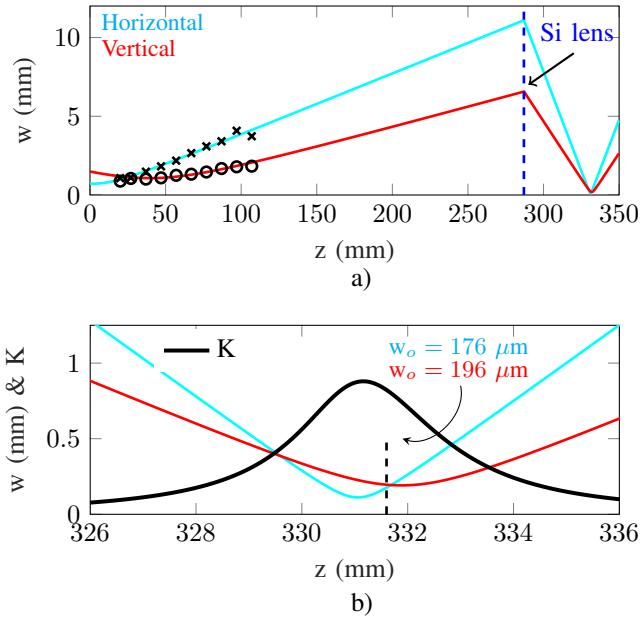

Fig. 7: Coupling efficiency. Simulation of the beam propagation in the current setup with a f = 38.1 mm silicon lens. a) Markers indicate beam radii measurements in both horizontal and vertical directions. b) Close-up of the focused beam, along with the coupling efficiency K.

18 K, where the emission frequency is 3.407 THz. Note that the QCL was driven in continuous-wave (cw) operation.

B. Coupling efficiency

To optimize the coupling of LO power from the QCL to the mixer, the QCL beam profile was measured at different positions along the optical axis z, starting from the QCL vacuum window, using a microbolometer camera. The measured beam radii in horizontal and vertical directions are indicated by markers in Fig. 7a along with the Gaussian fit. Note the different divergence angles ($\Theta = 0.22°$ and $1.5°$, respectively).

Based on those beam parameters and quasi-optical beam transformation by a thin lens, we have optimized the coupling efficiency K taking into account the mismatch of waist radii as well as waist offsets along the optical axis [26]. Due to the asymmetric profile of the QCL beam, the maximum achievable coupling efficiency is 88%. With $f = 38.1$ mm, the optimum coupling is achieved with the lens placed at $z = 287$ mm, cf. Fig. 7a. A close-up of the focused beam, along with the coupling efficiency, is shown in Fig. 7b. To verify the calculations for the transformed beam, the focused beam was measured with a microbolometer camera, as shown in Fig 8. The measured beam radii agree very well with the simulations at 331.6 mm (cf. marked position in Fig. 7b). Note that this position, with a rather symmetric beam, does not correspond to the maximum coupling efficiency. In conclusion, taking into account the maximum coupling efficiency of a pyramidal horn of 85% [26], a total of 75% of the incident QCL power is coupled in the mixer.

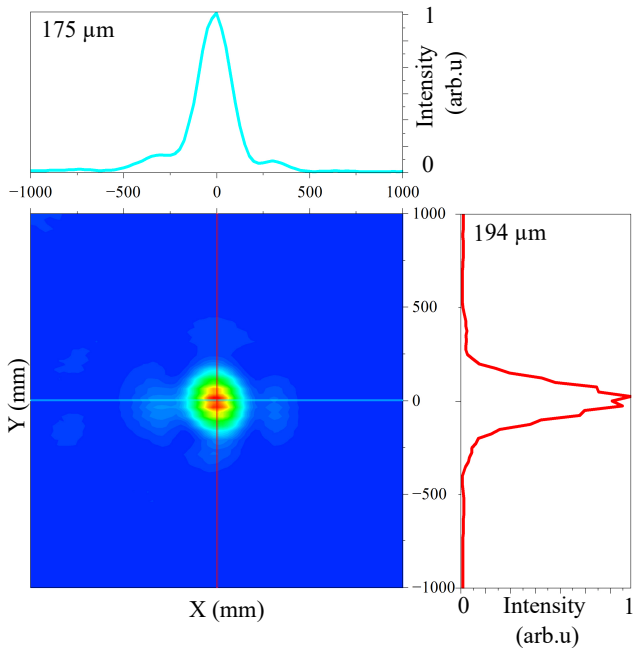

Fig. 8: Beam pattern of the QCL. Measured intensity at the focal point after the external Si lens.

C. Atmospheric transmission

Atmospheric transmission of a 1-m path at 1.135 mbar and 42% relative humidity at room temperature is shown in Fig.9. This model is based on the HITRAN data catalog [37]. The hydroxyl radical (OH) has a rotational transition at 3.551 THz; however, at this frequency, only 50% of the signal is transmitted, and the rest is absorbed due to atmospheric loss. To avoid this, a QCL operating at a different frequency is selected to maximize signal transmission. At 3.407 THz, signal transmission of about 87% is attainable for a 1-m path length. Consequently, the 331 mm optical path in our setup transmits ≈95% of the QCL power.

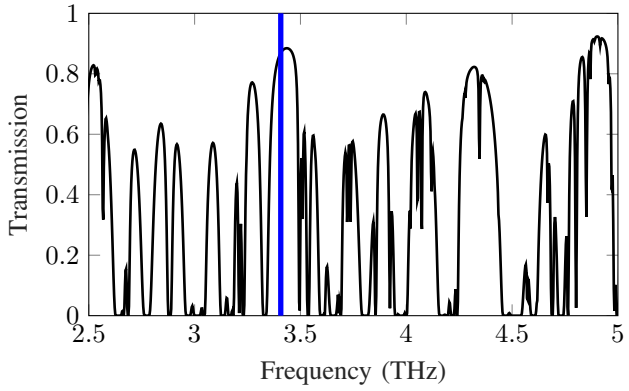

Fig. 9: Atmospheric transmission model. Estimated transmission for 1-m path at 1.135 mbar and 42% relative humidity at room temperature. At 3.407 THz, 87% of the signal is transmitted.

D. Beam splitter characterization

For combining the LO and RF signals, we use a thin Mylar film as a beam splitter. Mylar is the trade name of DuPont for Polyethylene terephthalate (PET) film. It has a refractive index of 1.72 and exhibits a notable absorption feature at 4.2 THz [38]. We have tested Mylar beam splitters with different thicknesses using an absolute power meter, and the relative reflection and transmission ratios for each film in s-plane polarization are summarized in the Table I. Fig. 10 shows the measured reflection values in black markers, along with simulations at 3.4 THz in the s- and p-planes, assuming a refractive index of 1.7 and a tilt angle of 45°. The absolute power measurements agree well with the simulations. However, for thicker films, the values deviate more strongly from the simulations because of increasing absorption, which was not included in the simulations.

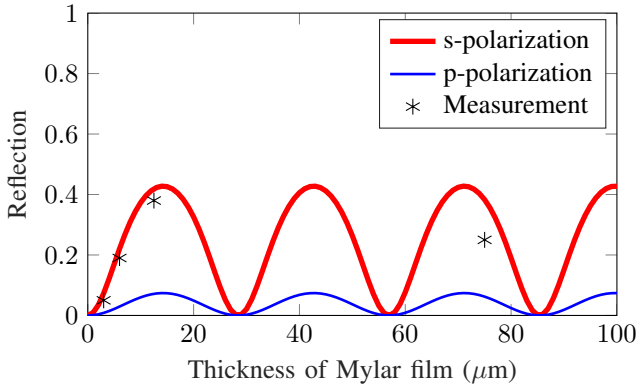

Fig. 10: Mylar beamsplitter. Simulated reflection versus Mylar film thickness at 3.4 THz in the s- and p-plane for refractive index of 1.7 and a tile angle of 45°. Markers indicate the reflected power measured using a TK power meter.

E. Power coupled to the mixer

From the 23 mW of QCL cw output power measured at the output window, 19 mW of power was measured at the interface (b-b') at $z = 33$ cm, refer to Table. II. Accordingly, approximately 83% of the power is transmitted through the air and the Si lens. With a wire grid polarizer set to 90° and 0°, an absolute power of 13.7 mW and 5.3 mW was measured in the E- and H-plane of the mixer, respectively. In conclusion, the power coupled into the mixer after reflection at the Mylar films is summarized in Table I.

TABLE I: Total power coupled to the mixer for the setup with 4 different Mylar films. Losses from imperfect coupling, the Si-lens, and the polarization mismatch are included in the measurements and estimations, respectively.

Mylar thickness (μm)	Relative transmission (%)	Relative reflection (%)	Coupled power (mW)
3	91%	5%	0.7 mW
6	70%	19%	1.9 mW
12.5	50%	38%	3.8 mW
75	41%	25%	2.5 mW

TABLE II: Measured cw power at different interfaces for QCL operating point: 550 mA and 18 K.

Interface	Measured Power
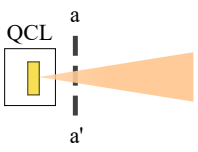	Total: 23 mW
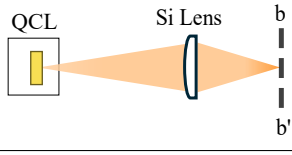	Total: 19 mW Pol 90°: 13.7 mW Pol 0°: 5.3 mW
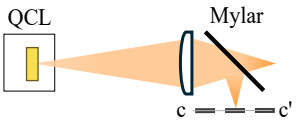	For 6-μm Mylar Total: 3.6 mW Pol 90°: 2.6 mW Pol 0°: 1 mW
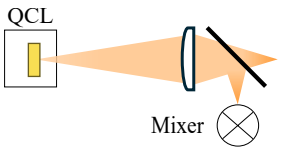	For 6-μm Mylar $2.6 \times 0.75 = 1.9$ mW Refer Section III-B

IV. Measurement Setup

In this section, we describe the experimental setup used to characterize the video responsivity and noise temperature of the mixers.

A. Video responsivity

To estimate the video response of the mixers, the voltage difference with and without the input THz signal from the QCL was measured at a fixed current [39]. The mixer is mounted on a three-axis Thorlabs micro manipulator stage vertically (i.e., *E*-plane split of the mixer block is perpendicular to the optical bench), and the mixer is biased using a bias-tee. A simplified schematic of the experimental setup is shown in the inset of Fig. 13. The emission from the QCL is focused on the mixer using a Si lens with f = 38.1 mm. The distance between the cryocooler housing and the mixer is approximately 33 cm. A mechanical chopper at 15 Hz, referenced to the lock-in amplifier, is used to modulate the video signal response of the mixers.

B. Noise temperature

The noise temperature measurements are carried out using the standard Y-factor technique on the full receiver, including the beam splitter and atmospheric losses, as well as the contribution from the bias-tee and IF amplifier chain. The Y-factor measurement was carried out using hot/cold calibration loads made of Eccosorb. A four-quadrant mechanical chopper with two quadrants lined with a flat piece of Eccosorb is used as the hot load placed at an ambient temperature of 296 K. The cold calibration load, consisting of 8-mm-thick Eccosorb and cooled to 77 K by liquid nitrogen, is housed

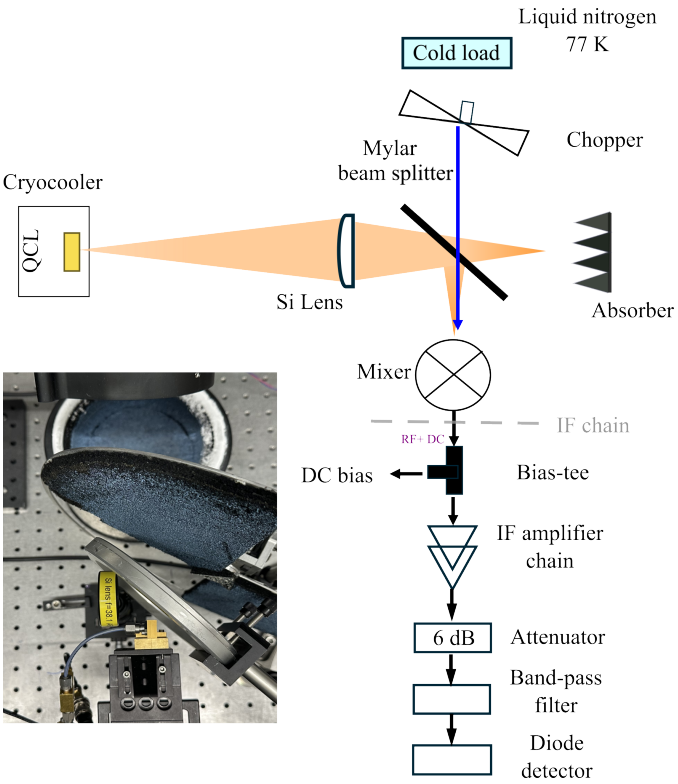

Fig. 11: RF measurement setup. Schematic of the noise temperature measurement setup showing the spatial diplexing of the RF (transmission) and LO signal (reflection) using a Mylar beamsplitter to the WM-57 mixer. Inset: Photograph of the measurement setup. The free-space path length for RF is about 15-20 cm, and LO is 33 cm. Note: Schematic is not to scale.

in a 15 cm aperture Dewar. A gold-plated mirror aligned at 45° directs the beam from the liquid nitrogen bath through the open ports of the mechanical chopper to the mixer under test. To avoid standing waves between the calibration load and the mixer, the chopper is aligned at an angle ($\approx 20°$) with respect to the orthogonal plane of the mixer. A temperature and humidity sensor was positioned near the experimental setup. Throughout the testing period, the ambient temperature fluctuated between 20 and 23°C, while relative humidity remained around 40–45%, typical of a standard laboratory environment. The Rayleigh-Jeans approximation was used to calculate the receiver noise temperature.

The incoming THz signal from the QCL is focused using a Si lens with a focal length of 38.1 mm as described above. A Mylar beam splitter positioned at 45° enables spatial multiplexing of the RF and LO signals, directing them to the mixer with an integrated pyramidal horn. In the configuration shown in Fig. 11, the reflected LO signal from the QCL is fed to the fundamental mixer, whereas the transmitted LO signal is absorbed using Eccosorb. The RF signal from the hot/cold load is coupled to the mixer in transmission mode.

For high-resolution spectroscopy measurements, the transmitted LO signal can be coupled to a harmonic mixer pumped by a solid-state multiplier chain, and the generated IF signal can be used to phase-lock the QCL [40].

C. IF chain

The IF amplifier chain consists of the following components. A dc-bias path for the mixer is provided through a bias-tee. The bias box is a custom-built analog dc power supply with a 1 mA current safety limit and additional protection against noise pickup.

The first-stage low-noise amplifier (LNA) is a low-noise factory LNF LNC, 0.2-3A, s/n 2230 Z [41]. At 296 K, it has a gain of 27 dB and an equivalent noise temperature of 30 K at 1.5 GHz. Followed by Miteq LNA-30-0010040013-10P LNA with 37 dB gain at 1.5 GHz and Mini-circuit ZX60-83LN-S+ LNA with 22 dB gain at 1.5 GHz. To operate at different intermediate frequencies, a band-pass filter (BPF) was used. Noise temperature measurements are performed at two intermediate frequencies, and the specifications are summarized below.

TABLE III: Band-pass filter specification

Specification	Frequency range	Center frequency	Bandwidth
VBF 1525+	1480-1570 MHz	1.525 GHz	90 MHz
ZX75BP-2150	2050-2250 MHz	2.15 GHz	200 MHz

This setup enables accurate noise-temperature measurements using a lock-in detector referenced to the 15-Hz chopper frequency, which extracts the output-power variation of the hot/cold load from a diode detector (8471E). To control the power level at the diode detector, a 6-dB SMA attenuator operating from DC to 6 GHz was placed between the last-stage LNA and the band-pass filter. Linearity of the amplifiers was checked by connecting a 3-dB SMA attenuator, which produced no observable change in the measured noise temperature. The IF chain's (see Fig. 11) noise temperature (T_{IF}) was determined by terminating the RF/dc port of the bias-tee along with the access cable to a 50-Ω load and measuring the corresponding power level at room temperature and at 77 K by immersing it in the liquid-nitrogen bath. Yielding a T_{IF} of 108 ± 10 K.

D. Mixer conversion loss

The mixer conversion loss (L_m) and mixer noise temperature (T_m) are determined by measuring the variation of receiver noise temperature for different T_{IF}, according to [42].

$$T_{Rec} = T_m + L_m T_{IF} \tag{1}$$

SMA attenuators (1 and 2 dB) were placed in the IF chain to vary (T_{IF}). From the measured DSB receiver noise temperature (T_{Rec}) corresponding to each T_{IF}, the parameters L_m and T_m were determined using a linear least-squares fit.

V. Results and Discussion

Two $In_{0.22}Ga_{0.78}As$ diodes integrated on an InP substrate with an anode diameter of 0.5 μm were assembled in E-plane split blocks. First, *I-V* characterization of the mixers was carried out. Followed by the RF characterization, which includes video responsivity and DSB receiver noise temperature measurements.

A. DC characterization

The dc test provides a useful diagnostic for the assembled mixers. IV curves of the assembled devices are obtained to verify that assembly has not degraded device quality. Table IV summarizes the extracted diode parameters for the devices under test, and the measured *I-V* response of the two mixers is presented in Fig. 12. The lower barrier of the $In_{0.22}Ga_{0.78}As$ diode can be noted in the higher saturation current (I_{sat}) of the diodes since the I_{sat} increases exponentially with the decreasing Φ_b [43].

TABLE IV: Extracted dc-parameters of the $In_{0.22}Ga_{0.78}As$ diode

Parameters	Mixer 1	Mixer 2
Series resistance $R_s(\Omega)$	40	39
Ideality factor η	1.25	1.27
Saturation current I_{sat} (pA)	4.5	4.4

B. RF characterization

The mixer is carefully aligned to achieve an optimum video response, as shown in Fig. 13. Mixer 2 exhibits a higher video response of 237 mV than mixer 1, which has a response of 215 mV at 0.31 V bias voltage. These values were measured with a lock-in amplifier with 1-s integration time and correspond to peak-to-peak signals of 521 mV for mixer 1 and 473 mV for mixer 2, respectively [44]. The power coupled to the mixer is about 10.3 mW in this setup, as shown in the inset of Fig. 13. The peak video responsivity of the mixers is about 51 V/W and 46 V/W, respectively. The two InGaAs mixers have an integrated pyramidal horn that is sensitive only to linear polarization, owing to its single-mode operation. To confirm that the mixers detect only the vertical component of the laser's polarization, the peak video output of mixer 1 was recorded with a 90°-oriented wire-grid polarizer in place and then without the polarizer. The measured video signals were 212 mV and 215 mV, respectively; the slight reduction in video signal with the polarizer can be attributed to the losses of the wiregrid polarizer.

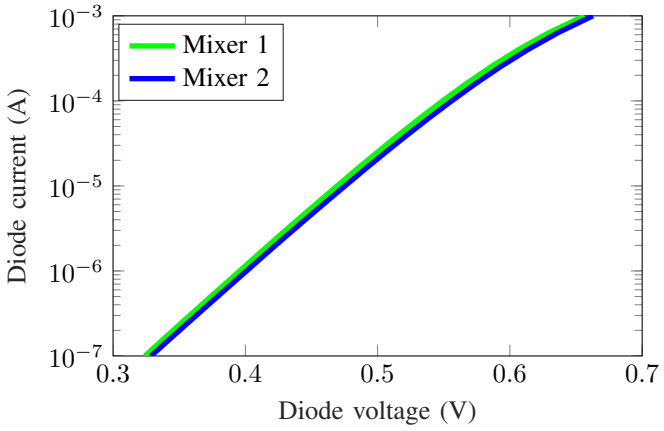

Fig. 12: Mixer diode dc-characteristics. Measured current-voltage response of the two $In_{0.22}Ga_{0.78}As$ diode mixers at room temperature.

Next, noise temperature measurements were carried out as shown in Fig. 11, and the measured uncorrected DSB receiver noise temperature of two $In_{0.22}Ga_{0.78}As$ mixers versus current bias are shown in Fig. 14a and b. Both mixers were measured at two intermediate frequencies, approximately 1.5 GHz and 2.1 GHz, which can be selected based on the BPFs. For each of these four configurations, measurements were performed with three Mylar beam splitters of different thicknesses: 6, 12.5, and 75 μm. For the 3 μm Mylar beam splitter, only 5% of the QCL power is reflected, and the power coupled to the mixer is about 0.7 mW (refer to Table I), which was insufficient to adequately pump the mixer, thereby resulting in high noise temperature $>$ 100 000 K at bias current 0.9 mA. In Fig. 5, the mixer conversion loss increases below 1 mW of available LO power at the anode.

Mixer 2 has the best DSB receiver noise temperature measured at room temperature, 28 500 K, at 3.407 THz. This result was obtained for a bias current of 0.9 mA, an IF of 1.5 GHz, a BPF bandwidth of 90 MHz, and with 6-μm Mylar, yielding 1.9 mW of coupled power to the mixer and 70% transmission from the hot/cold load. In the same operating conditions, Mixer 1 has about 32 000 K. For thicker Mylar films (12.5 μm and 75 μm), the power coupled to the mixer is 3.8 and 2.5 mW, respectively, but the hot/cold load transmission is lower, about 50% and 41%, respectively, which results in higher noise temperature.

Despite comparable extracted electrical parameters for both mixers, as shown in the table IV, Mixer 2 has a better performance. Video responsivity measurements further support this: Mixer 2 exhibits a lock-in video signal of 237 mV at a bias voltage of 0.3 V, whereas Mixer 1 reaches only 215 mV under identical conditions. By varying the IF chain noise temperature, the following parameters were determined: L_m of 16.7 $\pm$ 0.1 dB and T_m of 24 400 $\pm$ 400 K at bias current 0.9 mA as shown in Fig. 15.

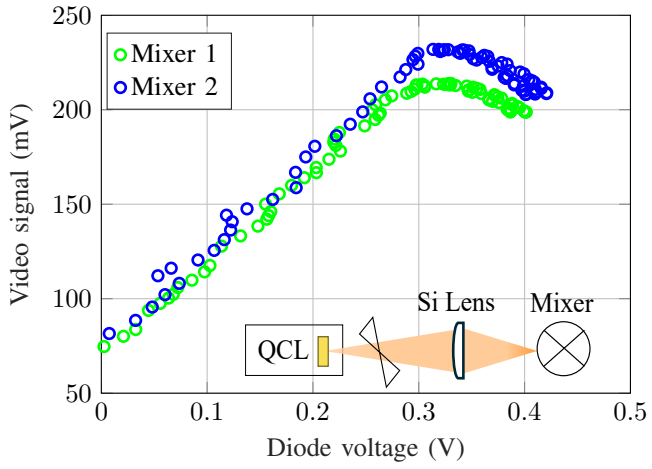

Fig. 13: Video responsivity measurements. The video signal response of two $In_{0.22}Ga_{0.78}As$ mixers versus bias voltage. Inset: Schematic of the experimental setup (not to scale). The peak video responsivity of the mixers is 51 V/W and 46 V/W, respectively.

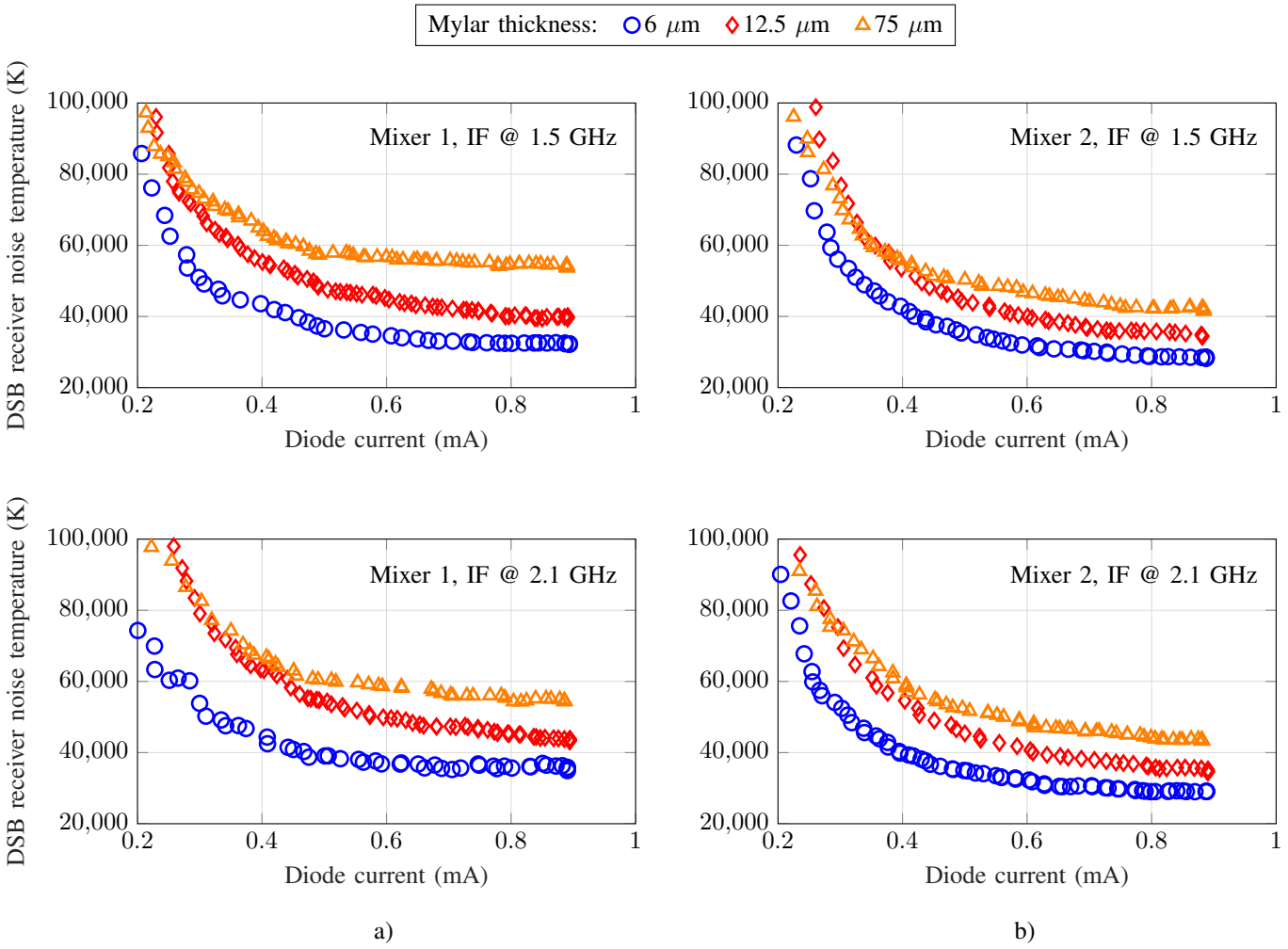

Fig. 14: DSB receiver noise temperature measurements. Uncorrected DSB T_{rec} versus current of two mixers (Mixer 1 and Mixer 2) at two different intermediate frequencies of about 1.5 and 2.1 GHz, with bandwidth of 90 MHz and 200 MHz. For each case, Mylar beam splitters with different thicknesses: 6 μm, 12.5 μm, and 75 μm were studied. The LO power coupled to the mixer is given in the Table I. The QCL was operated with a current bias of 550 mA and a temperature of 18 K. An uncorrected DSB T_{rec} of 28 500 K was measured for mixer 2 at 1.5 GHz, and the corresponding DSB T_{rec} with atmospheric correction for the cold load is 27 600 K.

State-of-the-art THz receivers with planar integrated Schottky diode mixers are summarized in Table V. The brightness temperature of the cold load is corrected for the atmospheric attenuation, which yields a DSB receiver noise temperature of 27 600 K for mixer 2 at 1.5-GHz IF. Note: some of the prior works cited in the table account for atmospheric attenuation and/or additional contributions such as lens-induced losses.

C. Model validation

To better understand the significantly higher conversion loss than the initially predicted 7 dB, refer to section II-A, HB simulations were conducted to analyze the discrepancy. The Champlin model for capturing the carrier inertia effects of a diode as lumped elements is included [45]. Although we are close to the plasma resonance in the device ($\approx$ 7.9 THz), the dominant factor is the increase in the series resistance of the undepleted, lightly doped epitaxial layer. An R_s of 70 Ω is calculated and applied to the HB simulation along with junction capacitance of $C_j = 0.6\ fF$ and parameters extracted from the dc measurements, refer to Table IV. As shown in Fig. 15, a reasonable fit at higher dc bias can be achieved with this straightforward approach.

VI. Conclusion

We have demonstrated 3.4-THz $In_{0.22}Ga_{0.78}As$ Schottky-barrier diode-based mixers with state-of-the-art DSB receiver noise temperature of 28 500 K and DSB mixer conversion loss of about 17 dB. The LO signal from the QCL and the RF signal were coupled via a Mylar beam splitter, yielding a compact receiver breadboard. We have characterized two mixers with different Mylar beam splitters at two IF frequencies. The mixers exhibit consistent and repeatable performance at 3.4 THz. To operate the mixers at 4.7 THz, it is important to

TABLE V: State-of-the-art THz receivers based on planar, integrated Schottky-barrier diode technology.

Frequency	Mission	Topology	Material	n-layer doping concentration (cm^{-3})	DSB receiver noise temperature at 296 K	Reference
3.4 THz		Single-ended	$In_{0.22}Ga_{0.78}As$	5×10^{17}	27 600 K	**This work**
2.5 THz	EOS-MLS	Single-ended	GaAs	1×10^{18}	16 500 K	[46]
2.06 THz	TLS-Dynamic*	Anti-parallel	GaAs	5×10^{17}	4 500 K	[11]
1.2 THz	JUICE-SWI	Anti-parallel	GaAs	3×10^{17}	2 500 K @ 128 K	[8]
1.2 THz		Anti-parallel	GaAs	3×10^{17}	2 000 K	[9], [47]
874 GHz	ISMAR	Anti-parallel	GaAs	3×10^{17}	3300 K	[7]
600 GHz	JUICE-SWI	Anti-parallel	GaAs	3×10^{17}	1100 K	[9]
600 GHz		Anti-parallel	GaAs	3×10^{17}	1000 K	[48]

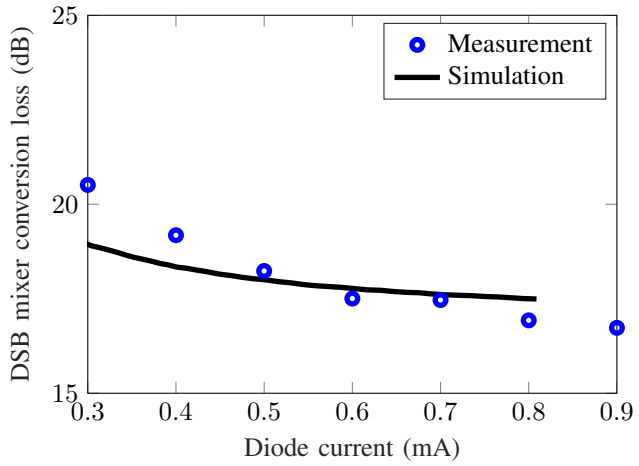

Fig. 15: Conversion loss. Estimated DSB mixer conversion loss for noise temperature measurement of Mixer 2 at 1.5 GHz IF. Harmonic-balance simulation includes the losses in the buffer region.

have a smaller anode to reduce the junction capacitance by incorporating planar air-bridged diode geometry. The successful demonstration of these mixers is a key step towards the realization of compact THz front-end systems, see Fig. 1. This is crucial for limb-sounding missions such as Keystone[1], which is crucial for detecting hydroxyl radicals in the mesosphere and lower thermosphere of Earth's atmosphere.

ACKNOWLEDGEMENT

The authors would like to thank K. Biermann, X. Lü, and L. Schrottke (PDI) for the design and fabrication of the QCL. Thanks to M. Wienold (DLR) for the micro-QCL optics design and fruitful discussions. Also, we thank A. Sahm and K. Paschke from the Ferdinand-Braun-Institut (FBH), Berlin, for assembling the micro QCL optical test bench. The authors would like to thank the VDI staff for the high-precision machining of mixer blocks.

[1]EOB - MLS NASA's Earth Observing Systems - Microwave Limb Sounder, JUICE - JUpiter ICy moon Explorer - Submillimeter Wave Instrument, ISMAR - International Sub-Millimeter Airborne Radiometer, Terahertz Limb Sounder TLS/Dynamic - Future planned NASA mission, Keystone - ESA selected Earth explorer mission

While writing this article, our esteemed colleague and friend Jeffrey Hesler has unfortunately passed away. His contributions to this field and his friendship were invaluable, and his presence is greatly missed by all of us. We wish to dedicate this work to him [49].

REFERENCES

[1] I. Mehdi, J. V. Siles, C. Lee, and E. Schlecht, "THz Diode Technology: Status, Prospects, and Applications," *Proceedings of the IEEE*, vol. 105, no. 6, pp. 990–1007, June 2017, DOI: 10.1109/JPROC.2017.2650235.

[2] H. Richter, C. Buchbender, R. Güsten, R. Higgins, B. Klein, J. Stutzki, H. Wiesemeyer, and H.-W. Hübers, "Direct measurements of atomic oxygen in the mesosphere and lower thermosphere using terahertz heterodyne spectroscopy," *Commun. Earth Environ.*, vol. 2, no. 1, Jan. 2021, DOI: 10.1038/s43247-020-00084-5.

[3] M. Wienold, A. D. Semenov, E. Dietz, S. Frohmann, P. Dern, X. Lü, L. Schrottke, K. Biermann, B. Klein, and H.-W. Hübers, "OSAS-B: A Balloon-Borne Terahertz Spectrometer for Atomic Oxygen in the Upper Atmosphere," *IEEE Trans. THz Sci. Technol.*, vol. 14, no. 3, p. 327–335, May 2024, DOI: 10.1109/TTHZ.2024.3363135,.

[4] P. B. Hansen, M. Wienold, and H.-W. Hübers, "Feasibility of a space-borne terahertz heterodyne spectrometer for atomic oxygen and temperature in the mesosphere and lower thermosphere," *Atmos. Meas. Tech.*, vol. 18, no. 20, p. 5749–5762, Oct. 2025, DOI: 10.5194/amt-18-5749-2025.

[5] U. Frisk, M. Hagström, J. Ala-Laurinaho, S. Andersson, J.-C. Berges, J.-P. Chabaud, M. Dahlgren, A. Emrich, H.-G. Florén, G. Florin, M. Fredrixon, T. Gaier, R. Haas, T. Hirvonen, Å. Hjalmarsson, B. Jakobsson, P. Jukkala, P. S. Kildal, E. Kollberg, J. Lassing, A. Lecacheux, P. Lehikoinen, A. Lehto, J. Mallat, C. Marty, D. Michet, J. Narbonne, M. Nexon, M. Olberg, A. O. H. Olofsson, G. Olofsson, A. Origné, M. Petersson, P. Piironen, R. Pons, D. Pouliquen, I. Ristorcelli, C. Rosolen, G. Rouaix, A. V. Räisänen, G. Serra, F. Sjöberg, L. Stenmark, S. Torchinsky, J. Tuovinen, C. Ullberg, E. Vinterhav, N. Wadefalk, H. Zirath, P. Zimmermann, and R. Zimmermann, "The Odin satellite," *Astron. Astrophys.*, vol. 402, no. 3, pp. L27–L34, Apr. 2003, DOI: 10.1051/0004-6361:20030335.

[6] S. Gulkis, M. Frerking, J. Crovisier, G. Beaudin, P. Hartogh, P. Encrenaz, T. Koch, C. Kahn, Y. Salinas, R. Nowicki, R. Irigoyen, M. Janssen, P. Stek, M. Hofstadter, M. Allen, C. Backus, L. Kamp, C. Jarchow, E. Steinmetz, A. Deschamps, J. Krieg, M. Gheudin, D. Bockelée-Morvan, N. Biver, T. Encrenaz, D. Despois, W. Ip, E. Lellouch, I. Mann, D. Muhleman, H. Rauer, P. Schloerb, and T. Spilker, "MIRO: Microwave Instrument for Rosetta Orbiter," *Space Sci. Rev.*, vol. 128, no. 1-4, pp. 561–597, Nov. 2007, DOI: 10.1007/s11214-006-9032-y.

[7] A. Hammar, P. Sobis, V. Drakinskiy, A. Emrich, N. Wadefalk, J. Schleeh, and J. Stake, "Low noise 874 GHz receivers for the international submillimetre airborne radiometer (ISMAR)," *Review of Scientific Instruments*, vol. 89, no. 5, p. 055104, May 2018, DOI: 10.1063/1.5017583.

[8] J. Treuttel, L. Gatilova, S. Caroopen, A. Feret, G. Gay, T. Vacelet, J. Valentin, Y. Jin, A. Cavanna, K. F. Jacob, S. Mignoni, V. Lavignolle, J.-M. Krieg, C. Goldstein, F. Courtade, C. Larigauderie, A. Ravanbakhsh, J.-P. Garcia, A. E. Maestrini, and P. Hartogh, "1200 GHz High Spectral Resolution Receiver Front-End of Submillimeter Wave Instrument for JUpiter ICy Moon Explorer: Part I - RF Performance

Optimization for Cryogenic Operation," *IEEE Trans. THz Sci. Technol.*, vol. 13, no. 4, pp. 324–336, 2023, DOI: 10.1109/TTHZ.2023.3263623.

[9] P. Sobis, V. Drakinskiy, N. Wadefalk *et al.*, "SWI 1200/600 GHz highly integrated receiver front-ends," in *Proceedings of the 36th ESA Antenna Workshop on Antennas and RF Systems for Space Science*. Noordwijk, The Netherlands: ESA/ESTEC, 2015.

[10] P. Eriksson, A. Emrich, K. Kempe, J. Riesbeck, A. Aljarosha, O. Auriacombe, J. Kugelberg, E. Hekma, R. Albers, A. Murk, S. Møller Pedersen, L. John, J. Stake, P. McEvoy, B. Rydberg, A. Dybbroe, A. Thoss, A. Canestri, C. Accadia, P. Colucci, D. Gherardi, and V. Kangas, "The arctic weather satellite radiometer," *Atmospheric Measurement Techniques*, vol. 18, no. 18, p. 4709–4729, Sep. 2025, DOI: 10.5194/amt-18-4709-2025.

[11] A. E. Maestrini, J. V. Siles, C. Lee, R. Lin, and I. Mehdi, "A 2 THz Room Temperature Bias-Able Schottky Mixer," *IEEE Trans. THz Sci. Technol.*, vol. 15, no. 2, pp. 169–180, 2025, DOI: 10.1109/T-THZ.2024.3472294.

[12] M. Anderberg, P. Sobis, V. Drakinskiy, J. Schleeh, S. Dejanovic, A. Emrich, and J. Stake, "A 183-GHz Schottky Diode Receiver with 4 dB Noise Figure," in *2019 IEEE MTT-S International Microwave Symposium (IMS)*, 2019, pp. 172–175, DOI: 10.1109/MWSYM.2019.8701051.

[13] P. J. Sobis, N. Wadefalk, A. Emrich, and J. Stake, "A broadband, low noise, integrated 340 GHz Schottky diode receiver," *IEEE Microw. Wireless Compon. Lett*, vol. 22, no. 7, pp. 366–368, July 2012, DOI: 10.1109/LMWC.2012.2202280.

[14] P. F.-X. Neumaier, H. Richter, J. Stake, H. Zhao, A.-Y. Tang, V. Drakinskiy, P. Sobis, A. Emrich, A. Hulsmann, T. K. Johansen, T. Bryllert, J. Hanning, V. Krozer, and H.-W. Hubers, "Molecular Spectroscopy With a Compact 557-GHz Heterodyne Receiver," *IEEE Trans. THz Sci. Technol.*, vol. 4, no. 4, p. 469–478, Jul. 2014, DOI: 10.1109/t-thz.2014.2326554.

[15] B. Thomas, A. Maestrini, and G. Beaudin, "A low-noise fixed-tuned 300-360-GHz sub-harmonic mixer using planar Schottky diodes," *IEEE Microw. Wireless Compon. Lett*, vol. 15, no. 12, pp. 865–867, 2005, DOI: 10.1109/LMWC.2005.859992.

[16] J. Treuttel, L. Gatilova, A. Maestrini, D. Moro-Melgar, F. Yang, F. Tamazouzt, T. Vacelet, Y. Jin, A. Cavanna, J. Matéos, A. Féret, C. Chaumont, and C. Goldstein, "A 520–620-GHz Schottky Receiver Front-End for Planetary Science and Remote Sensing With 1070 K–1500 K DSB Noise Temperature at Room Temperature," *IEEE Trans. THz Sci. Technol.*, vol. 6, no. 1, pp. 148–155, 2016, DOI: 10.1109/TTHZ.2015.2496421.

[17] M. C. Gaidis, H. M. Pickett, P. H. Siegel, C. D. Smith, R. P. Smith, and S. C. Martin, "A 2.5 THz receiver front-end for spaceborne applications," in *1998 IEEE Sixth International Conference on Terahertz Electronics Proceedings. THZ 98. (Cat. No.98EX171)*, Sep. 1998, pp. 13–17, DOI: 10.1109/THZ.1998.731652.

[18] E. Schlecht, J. V. Siles, C. Lee, R. Lin, B. Thomas, G. Chattopadhyay, and I. Mehdi, "Schottky Diode Based 1.2 THz Receivers Operating at Room-Temperature and Below for Planetary Atmospheric Sounding," *IEEE Trans. THz Sci. Technol.*, vol. 4, no. 6, pp. 661–669, 2014, DOI: 10.1109/TTHZ.2014.2361621.

[19] D. Jayasankar, N. Rothbart, H. Richter, V. Drakinskiy, P. Sobis, H.-W. Hübers, and J. Stake, "Design and characterisation of a 3.5-THz fundamental Schottky mixers," in *Proceedings of the 32nd International Symposium on Space Terahertz Technology (ISSTT)*, Baeza, Spain, Oct. 2022.

[20] J. Zmuidzinas and P. Richards, "Superconducting detectors and mixers for millimeter and submillimeter astrophysics," *Proceedings of the IEEE*, vol. 92, no. 10, pp. 1597–1616, 2004, DOI: 10.1109/JPROC.2004.833670.

[21] D. Jayasankar, A. Koj, J. Hesler, and J. Stake, "Impact of E-Plane Misalignment on THz Diagonal Horn Antennas," *IEEE Trans. THz Sci. Technol.*, vol. 15, no. 2, pp. 143–150, 2025, DOI: 10.1109/T-THZ.2024.3449792.

[22] H. Ito and T. Ishibashi, "InP/InGaAs fermi-level managed barrier diode for broadband and low-noise terahertz-wave detection," *Japanese Journal of Applied Physics*, vol. 56, no. 1, p. 014101, Dec. 2016, DOI: 10.7567/jjap.56.014101.

[23] E. Schlecht and R. Lin, "Schottky Diode Mixers on Gallium Arsenide Antimonide or Indium Gallium Arsenide," in *Proceedings of the 19th International Symposium on Space Terahertz Technology*, Groningen, The Netherlands, Apr. 2008.

[24] T. Reck, N. Rothbart, D. Jayasankar, J. Hesler, J. Stake, and H.-W. Hübers, "Characterization of 3.4-4.7 THz Schottky Diode Mixers," in *2025 50th International Conference on Infrared, Millimeter, and Terahertz Waves (IRMMW-THz)*, 2025, pp. 1–2, DOI: 10.1109/IRMMW-THz61557.2025.11320125.

[25] W. Bishop, K. McKinney, R. Mattauch, T. Crowe, and G. Green, "A Novel Whiskerless Schottky Diode for Millimeter and Sub-millimeter Wave Application," in *1987 IEEE MTT-S International Microwave Symposium Digest*, vol. 2, 1987, pp. 607–610, DOI: 10.1109/MWSYM.1987.1132483.

[26] P. Goldsmith, "Quasi-optical techniques," *Proceedings of the IEEE*, vol. 80, no. 11, pp. 1729–1747, 1992, DOI: 10.1109/5.175252.

[27] J. Louhi, "The capacitance of a small circular Schottky diode for submillimeter wavelengths," *IEEE Microw. Guided Wave Lett.*, vol. 4, no. 4, pp. 107–108, Apr. 1994, DOI: 10.1109/75.282574.

[28] A. Y. Tang and J. Stake, "Impact of Eddy Currents and Crowding Effects on High-Frequency Losses in Planar Schottky Diodes," *IEEE Trans. Electron Device Lett.*, vol. 58, no. 10, pp. 3260–3269, Oct. 2011, DOI: 10.1109/TED.2011.2160724.

[29] S. Weinreb and A. Kerr, "Cryogenic cooling of mixers for millimeter and centimeter wavelengths," *IEEE Journal of Solid-State Circuits*, vol. 8, no. 1, pp. 58–63, 1973, DOI: 10.1109/JSSC.1973.1050345,.

[30] H. Nyquist, "Thermal agitation of electric charge in conductors," *Physical Review*, vol. 32, no. 1, p. 110–113, Jul. 1928, DOI: 10.1103/physrev.32.110.

[31] J. B. Johnson, "Thermal agitation of electricity in conductors," *Physical Review*, vol. 32, no. 1, p. 97–109, Jul. 1928, DOI: 10.1103/physrev.32.97.

[32] A. Der Ziel, "Theory of shot noise in junction diodes and junction transistors," *Proceedings of the IRE*, vol. 43, no. 11, p. 1639–1646, 1955, DOI: 10.1109/jrproc.1955.277990.

[33] R. Voigt, M. Wienold, X. Lü, L. Schrottke, K. Biermann, A. Sahm, K. Paschke, and H.-W. Hubers, "High-power micro-optical bench terahertz quantum-cascade laser system," *IEEE Trans. THz Sci. Technol.*, Oct. 2025, submitted.

[34] L. Schrottke, X. Lü, B. Röben, K. Biermann, T. Hagelschuer, M. Wienold, H.-W. Hübers, M. Hannemann, J. H. van Helden, J. Röpcke, and H. T. Grahn, "High-performance GaAs/AlAs terahertz quantum-cascade lasers for spectroscopic applications," *IEEE Trans. THz Sci. Technol.*, vol. 10, no. 2, pp. 133–140, Mar. 2020, DOI: 0.1109/T-THZ.2019.2957456.

[35] D. Jayasankar, V. Drakinskiy, N. Rothbart, H. Richter, X. Lü, L. Schrottke, H. T. Grahn, M. Wienold, H.-W. Hübers, P. Sobis, and J. Stake, "A 3.5-THz, $\times$6-Harmonic, Single-Ended Schottky Diode Mixer for Frequency Stabilization of Quantum-Cascade Lasers," *IEEE Trans. THz Sci. Technol.*, vol. 11, no. 6, pp. 684–694, 2021, DOI: 10.1109/T-THZ.2021.3115730.

[36] R. J. Wylde, *Installation and Operating Instructions for the TK Terahertz Absolute Power Meter System*, Thomas Keating Ltd., Billingshurst, West Sussex, United Kingdom, Nov. 2002. [Online]. Available: https://www.terahertz.co.uk/images/tki/PMETER/TKPOWERMETERMANUAL.pdf

[37] I. E. Gordon and et al., "The hitran2020 molecular spectroscopic database," *J. Quant. Spectrosc. Radiat. Transf.*, vol. 277, p. 107949, 2022, DOI: 10.1016/j.jqsrt.2021.107949,.

[38] E. Bründermann, H. Hübers, and M. Kimmitt, *Terahertz Techniques*, ser. Springer Series in Optical Sciences. Springer Berlin Heidelberg, 2012. [Online]. Available: https://books.google.de/books?id=obW5BQAAQBAJ

[39] A. Kreisler *et al.*, "Parameters influencing far infrared videodetection with submicron-size Schottky diodes," *International Journal of Infrared and Millimeter Waves*, vol. 5, no. 4, p. 559–584, Apr. 1984, DOI: 10.1007/bf01010152.

[40] H. Richter, N. Rothbart, M. Wienold, X. Lü, K. Biermann, L. Schrottke, D. Jayasankar, J. Stake, P. Sobis, and H.-W. Hübers, "Phase Locking of Quantum-Cascade Lasers Operating Around 3.5 and 4.7 THz With a Schottky-Diode Harmonic Mixer," *IEEE Trans. THz Sci. Technol.*, vol. 14, no. 3, pp. 346–353, 2024, DOI: 10.1109/TTHZ.2024.3385379.

[41] Lownoise Factory. (2024, aug) LNF LNC0-2 2/3B. Lownoise Factory. Accessed: 2026-01-07. [Online]. Available: https://lownoisefactory.com/product/lnf-lnc0-2_3b/

[42] R. Trambarulo and H. Berger, "Conversion loss and noise temperature of mixers from noise measurements," in *MTT-S International Microwave Symposium Digest*. MTT005, 1983, p. 364–365, DOI: 10.1109/mwsym.1983.1130913.

[43] E. Rhoderick, "Metal-semiconductor contacts," *IEE Proceedings I Solid State and Electron Devices*, vol. 129, no. 1, p. 1, 1982, DOI: 10.1049/ip-i-1.1982.0001.

[44] Stanford Research Systems, "About lock-in amplifiers," application Note AN-102 (rev. 1.2). [Online]. Available: https://www.thinksrs.com/downloads/pdfs/applicationnotes/AboutLIAs.pdf

[45] K. Champlin and G. Eisenstein, "Cutoff Frequency of Submillimeter Schottky-Barrier Diodes," *IEEE Trans. Microw. Theory Techn.*, vol. 26, no. 1, p. 31–34, Jan. 1978, DOI: 10.1109/tmtt.1978.1129302.
[46] P. H. Siegel, R. P. Smith, M. C. Gaidis, and S. C. Martin, "2.5-THz GaAs monolithic membrane-diode mixer," *IEEE Trans. on Microw. Theory Tech.*, vol. 47, no. 5, pp. 596–604, 1999, DOI: 10.1109/22.763161.
[47] P. Sobis, V. Drakinskiy, A. Emrich, J. Stake *et al.*, "Compact and Broadband 1200/600-GHz Schottky Barrier-Diode Receivers," *manuscript in preparation*, 2026.
[48] J. M. Treuttel, T. Thuroczy, A. Feret, G. Gay, L. Gatilova, T. Vacelet, C. Chaumont, E. Sernoux, P. Mondal, and J. Puech, "Demonstration of a 25% bandwidth 520-680 ghz schottky receiver front-end for planetary science and remote sensing," in *Millimeter, Submillimeter, and Far-Infrared Detectors and Instrumentation for Astronomy XI*. SPIE, Aug. 2022, p. 179, DOI: 10.1117/12.2630052.
[49] T. W. Crowe, S. H. Jones, J. Stake, I. Mehdi, and N. Llombart, "In Memoriam of Jeffrey L. Hesler," *IEEE Trans. THz Sci. Technol.*, vol. 16, no. 2, pp. 88–89, 2026, DOI: 10.1109/TTHZ.2026.3654821.

Divya Jayasankar was born in India in 1994. She received her bachelor's degree in electronics and communication engineering in 2015. Followed by a master's degree in wireless, photonics and space engineering and a PhD degree in terahertz electronics from Chalmers University of Technology, Sweden, in 2019 and 2024, respectively.

Since 2025, she has been working as a postdoctoral researcher at the German Aerospace Centre (DLR), Berlin, and as a guest researcher at the Terahertz and Millimeter wave Laboratory, Chalmers University of Technology, Sweden. During her PhD, she was a visiting student at DLR, University of Warwick, and Virginia Diodes Inc. (VDI). Her research interests include the development of THz heterodyne receiver systems for space/airborne missions and THz metrology.

D. Jayasankar received the Ericsson Research Foundation award, the European Microwave Association (EuMA) internship award, the IEEE-MTTs graduate fellowship, and the ARFTG Roger Pollard Student Memorial Fellowship in Microwave Measurement by the Advanced RF Techniques Group (ARFTG). In 2022, she also won second place in the best student paper competition at the ISSTT conference in Baeza, Spain. In 2023, she received a research grant from VINNOVA (Sveriges innovationsmyndighet) to conduct THz metrology research.

Theodore J. Reck (Senior Member, IEEE) received the B.S. degree from the University of Texas at Austin, Austin, TX, USA, in 2000 and the Ph.D. degree from the University of Virginia, Charlottesville, VA, USA, in 2010, both in electrical engineering. From 2010 to 2013, he was a NASA Postdoctoral Fellow with the Jet Propulsion Laboratory (JPL), developing silicon micromachined packaging for terahertz systems. From 2013 to 2018, he was a Member of the technical staff developing terahertz components and systems with JPL. In 2018, he joined Virginia Diodes Inc., Charlottesville, VA, as a Senior Engineer. His research interests include Schottky-diode mixers and multipliers, power-combining techniques, RF-MEMS, and terahertz metrology.

Nick Rothbart was born in Berlin, Germany, in 1985. He received the M.Sc. degree in physics from the Humboldt-Universität zu Berlin, Berlin, Germany, in 2011 and the Ph.D. (Dr. rer. nat.) degree in physics from the Technische Universität Berlin, Berlin, Germany, in 2015 for his involvement in THz imaging and spectroscopy that was accomplished at the German Aerospace Center (DLR), Berlin, Germany, and partially at the University of Massachusetts, Lowell, MA, USA, and supported by a scholarship and membership at Helmholtz Research School on Security Technologies. From 2014 to 2015, he was with the Federal Institute for Materials Research and Testing, Berlin, Germany. Since 2015, he has been involved in millimeter-wave/THz gas spectroscopy at DLR and the Humboldt-Universität zu Berlin.

Jan Stake (Fellow, IEEE) was born in Uddevalla, Sweden, in 1971. He received an M.Sc. in electrical engineering and a Ph.D. in microwave electronics from Chalmers University of Technology in Gothenburg, Sweden, in 1994 and 1999, respectively.

In 1997, he was a Research Assistant at the University of Virginia, Charlottesville, VA, USA. From 1999 to 2001, he was a Research Fellow with the Millimeter Wave Group at the Rutherford Appleton Laboratory, Didcot, UK. He then joined Saab Combitech Systems AB, Gothenburg, Sweden, as a Senior RF/microwave Engineer until 2003. From 2000 to 2006, he held different academic positions with the Chalmers University of Technology, and from 2003 to 2006, he was also the Head of the Nanofabrication Laboratory, Department of Microtechnology and Nanoscience (MC2). In 2006, he was appointed Professor and the Head of the Terahertz and Millimeter Wave Laboratory at Chalmers University of Technology. He was a Visiting Professor with the Submillimeter Wave Advanced Technology (SWAT) Group at Caltech/JPL, Pasadena, CA, USA, in 2007 and at TU Delft, the Netherlands, in 2020. He received an appointment as a visiting research fellow at the National Physical Laboratory, UK, in the year 2024. He is also the co-founder of Wasa Millimeter Wave AB, Gothenburg, Sweden. His research interests include high-frequency semiconductor devices, terahertz electronics, submillimeter wave measurement techniques, and terahertz systems.

Prof. Stake served as the Editor-in-Chief for the IEEE Transactions on Terahertz Science and Technology between 2016 and 2018 and as Topical Editor between 2012 and 2015. From 2019 to 2021, he was chairperson of the IEEE THz Science and Technology Best Paper Award committee. He served on the International Society of Infrared, Millimeter, and Terahertz Waves (IRMMW-THz) organization committee from 2017 to 2024.

Jeffrey Hesler (Fellow, IEEE) received the B.S.E.E. degree from Virginia Tech, Blacksburg, VA, USA, in 1989, and the M.S.E.E. and Ph.D. degrees from the University of Virginia, Charlottesville, VA, USA, in 1991 and 1996, respectively.

He is the president and Chief Technology Officer of Virginia Diodes Inc., Charlottesville, VA, USA, and a Visiting Research Assistant Professor at the University of Virginia. His career is focused on the creation of new technologies that are making possible the full exploitation of the Terahertz (THz) frequency band for scientific, defence, and industrial applications. He has authored and coauthored more than 150 technical papers in refereed international conferences and journals, given talks at THz-focused workshops and conferences such as IMS and EuMW. THz systems based on his innovative designs are now used in hundreds of research laboratories throughout the world. Dr. Hesler is a member of IEEE TC MTT-4 on THz Technology and Applications and serves as a reviewer for a variety of IEEE and IEE journals. In 2024, he became an Adjunct Professor at the Terahertz and Millimetre Wave Laboratory, Department of Microtechnology and Nanoscience (MC2), Chalmers University of Technology. He passed away in October 2025.

Heinz-Wilhelm Hübers received the Diplom and doctoral degrees in physics from the Universität Bonn, Bonn, Germany, in 1991 and 1994, respectively. From 1991 to 1994, he was with the Max-Planck-Institut für Radioastronomie, Bonn, Germany. In 1994, he joined the Deutsches Zentrum für Luft- und Raumfahrt (German Aerospace Center, DLR), Berlin, Germany, becoming the Head of Department in 2001. From 2009 to 2014, he was a Professor of Experimental Physics with the Technische Universität Berlin, Berlin, Germany, and the Head of the Department "Experimental Planetary Physics" at DLR. In 2014, he became the Director of the Institute of Optical Sensor Systems, DLR, and in 2024, Director of the Institute of Space Research in Berlin. In 2014, he was appointed as Professor at the Humboldt-Universität zu Berlin. His research interests include THz physics and spectroscopy, particularly in THz systems for astronomy, planetary research, and security. Prof. Hübers has received the Innovation Award on Synchrotron Radiation (2003) and the Lilienthal Award (2007). In 2021, he received an honorary doctorate at Chalmers University of Technology, Gothenburg, Sweden.